EVALUATION OF SYRINGIC ACID-LOADED BORONIC ACID FUNCTIONALIZED MESOPOROUS SILICA PROPERTIES

Simona IONITA[1], Mihaela DEACONU[2], Ionela Nicoleta IRIMESCU[3], Roxana Cristina POPESCU[4], Mona MIHAILESCU[5], Ana Maria SANDU[6], Mioara PRUNDEANU[7], Diana Iulia SAVU[8], Daniela BERGER[9]

Nanotechnology addresses a current issue in cancer treatment, the non-specificity of cytotoxic agents associated with severe side effects. Mesoporous silica-based systems emerged as promising drug delivery vehicles that can be modified to target tumoral cells in order to achieve a better therapeutic effect. Herein, MCM-41 silica was functionalized with a boronic acid derivative, as a targeting agent towards breast cancer cells, and loaded with syringic acid, a phenolic acid with a reported antitumoral potential. The resulting system's cytotoxicity and internalization into cells were evaluated on breast cancer cells and compared to human fibroblasts.

Keywords: mesoporous silica, 4-carboxyphenylboronic acid, syringic acid, internalization.

[1] PhD student., Department of Inorganic Chemistry, Physical-Chemistry & Electrochemistry, National University of Science and Technology POLITEHNICA of Bucharest, Romania, e-mail: simona.ionita2405@upb.ro

[2] PhD eng., CAMPUS Research Centre, National University of Science and Technology POLITEHNICA of Bucharest; e-mail: mihaela.deaconu@upb.ro

[3] PhD student, Applied Sciences Doctoral School, National University of Science and Technology POLITEHNICA of Bucharest; Tehnoplus Medical SRL, Bucharest, Romania

[4] PhD eng. Department of Life and Environmental Sciences, "Horia Hulubei" National Institute for Research and Development in Physics and Nuclear Engineering, Magurele, Romania; Department of Bioengineering and Biotechnology, National University of Science and Technology POLITEHNICA of Bucharest, Romania, e-mail: rcpopescu@nipne.ro

[5] Prof., Department of Physics, National University of Science and Technology POLITEHNICA of Bucharest Romania, e-mail: mona.mihailescu@upb.ro

[6] PhD eng., CAMPUS Research Centre, National University of Science and Technology POLITEHNICA of Bucharest, Romania, e-mail: ana_maria.sandu@upb.ro

[7] PhD eng., Department of Inorganic Chemistry, Physical-Chemistry &Electrochemistry, National University of Science and Technology POLITEHNICA of Bucharest, Romania.

[8] PhD eng., Department of Life and Environmental Sciences, "Horia Hulubei" National Institute for Research and Development in Physics and Nuclear Engineering, Magurele, Romania, e-mail: dsavu@nipne.ro

[9] Prof., Department of Inorganic Chemistry, Physical-Chemistry &Electrochemistry, National University of Science and Technology POLITEHNICA of Bucharest, Romania, e-mail: daniela.berger@upb.ro

1. Introduction

Cancer incidence is steadily increasing worldwide, being associated with not only environmental factors, but also a large number of internal factors, from impaired cellular function to mutations and oxidative stress [1-3]. Novel treatment options emerge as a need to solve the increasing concerns regarding drug resistance in cancer therapy, as well as to avoid the adverse effects of conventional chemotherapy. Phenolic compounds have emerged as compounds that can be used in cancer therapy, owing mainly to their antioxidant activity [4]. At the same time, there is an increasing interest in developing targeted drug delivery systems, which can selectively bind to receptors present in tumoral cells, overcoming the disadvantages of classical treatment options [5].

Using drug delivery systems as effective chemotherapeutic agents is a requirement that can be met by various nanoplatforms, such as liposomes, polymer micelles, iron oxide nanoparticles and mesoporous silica nanoparticles (MSN) [6]. The latter are among the most versatile carriers, as their specific surface area usually ranges up to 1000 m^2/g, possessing tunable properties, such as pore size and particle dimensions and shape, as well as an easily tailorable surface properties, owing to the presence of silanol groups [7].

Functionalization of MSN surface can be used to achieve both targeting and controlled delivery of a biomolecule towards the affected site [8-10]. Depending on the functional group characteristics, the loading capacity with biomolecules can be improved, agglomeration of the particles can be prevented, or the solubilization of biomolecules can be drastically enhanced [11]. Functional groups could also exhibit targeting capacity towards different receptors overexpressed by cancer cells. Such a moiety is boronic acid, which can target sialic acid receptors from the cancer cells surface [12-14]. Xu et al. prepared 4-carboxyphenylboronic (4-CPBA) acid-decorated micelles for co-delivery of camptothecin and gemcitabine and found an increased cellular internalization for the co-delivery system in MCF-7/ADR breast cancer cells [15]. MSN were also functionalized using 3-CPBA and capped with polyacrylic acid for the targeted delivery of cumin aldehyde in breast tumoral cells, resulting in induced apoptosis through mitochondrial damage and a reduction in growth of mammal tumor in female mice [16].

Phenolic compounds are gaining interest in biomedical field, owing to their antibacterial activity [17], antioxidant effect [18], and antitumoral properties [19]. Phenolic acids are usually derivatives of benzoic acid or cinnamic acid. Syringic acid is a benzoic acid derivative, naturally present in dates, grapes, mulberries or honey [20], exhibiting antitumoral potential against skin cancer [21], human colorectal cancer [22], and hamster buccal pouch carcinogenesis [23]. There is also evidence that syringic acid aids in suppressing breast cancer cell proliferation, when combined with another phytochemical, vitexin [24]. The

antidiabetic activity of syringic acid was tested on diabetic rats, resulting in a decrease in blood glucose towards normal concentrations [25]. Black mulberry extract, having syringic acid as major component, was shown to present antidepressant and neuroprotective effects on mice [26]. Moreover, embedding of syringic acid into a gelatin/ZnO nanocomposite led to anticancer activity against hepatocellular carcinoma [27].

In this study, 4-carboxyphenilboronic acid was bound to the surface of MCM-41 silica and compared to a composite consisting in 4-CPBA physically adsorbed onto aminopropyl-modified MCM-41 carrier. Syringic acid was loaded onto the boronic acid-functionalized carrier mesopores and its cytotoxic effect was tested *in vitro*, on both a breast tumoral cells (BT474) and a normal human cell line (BJ fibroblasts). It is possible to visualize the internalization of these nanoparticles in cells, in their natural environment, using a technique that records the light scattered on the nanometric details of the samples [28].

2. Experimental

All reagents used in this study were of analytical grade purchased from Sigma-Aldrich and were used as received.

2.1 Synthesis of mesoporous carriers modified with functional groups

Mesoporous silica nanoparticles were prepared according to the reference [17]. Two types of functionalized materials were obtained and denoted MCM-NH_2 and MCM-B, containing aminopropyl and 4-carboxyphenilboronic (4-CPBA) acid moieties, respectively. Briefly, a 40% wt. boronic acid derivative was adsorbed onto MCM-41 silica through impregnation technique. Afterwards, (3-aminopropyl)triethoxysilane (APTES) functionalization was conducted at reflux using 100 mg silica containing 4-CPBA, considering a 1/0.15 silica/APTES molar ratio, in 12 mL dry toluene, 15 h. The resulting solid was separated through centrifugation and washed with synthesis solvent, acetone, and ethanol, and labelled MCM-B. A similar procedure was used for MCM-NH_2, without 4-CPBA impregnation step. For comparison, one sample with CPBA adsorbed onto MCM-NH_2 carrier was also obtained and denoted as CPBA@MCM-NH_2.

2.2 Preparation of syringic acid-loaded samples

Syringic acid-containing composites were prepared using impregnation method, considering syringic acid/support mass ratio of 1/4 for both MCM-NH_2 and MCM-B materials. A 50 mg/mL methanolic solution of syringic acid was poured on vacuum dried silica-type supports.

2.3 Syringic acid release experiments

Syringic acid (SA) release experiments were carried out using a Shimadzu UV-1800 spectrophotometer. The phenolic acid release profiles and its dissolution

curve were acquired in phosphate buffer solution (PBS) pH 5.5, at 37°C, for 24 h, considering a maximum 300 µg/mL syringic acid concentration. The absorbance of the release medium was measured at 260 nm, quantifying syringic acid based on a standard curve ($y=0.047*x$, $R^2=0.9979$, in the concentration range of 1-25 µg/mL).

2.4 Characterization of materials

Structural characterization of the carriers was examined through small-angle and wide-angle X-ray diffraction (Rigaku Miniflex II equipment). FTIR spectra were measured in potassium bromide on a Bruker Tensor 27 spectrometer between 4000 to 400 cm^{-1} with 64 scans. Thermal analysis (TG-DTA) was performed with a Netzsch STA 2500 Regulus instrument, to determine the organic group content in the functionalized carriers. The samples were heated from 30°C to 800°C with 10°C/min rate, in synthetic air (50 mL/min). Scanning electron microscopy (SEM) images were recorded using a Tescan Vega 3 LMH microscope and employed to investigate the morphology of resulting materials. Nitrogen adsorption/desorption isotherms (Micromeritics Tristar II Plus) were recorded to study the porosity of boronic acid-functionalized sample. The BET method was used to determine the specific surface area from isotherms and the total pore volume was measured at relative pressure P/P_0 =0.99.

2.5 Cytotoxicity evaluation

Cellular viability was quantitatively determined (MTT assay) on human dermal BJ fibroblasts and on BT474 ductal breast carcinoma cells. The protocol of cytotoxicity evaluation was described in our previous paper [29]. In brief, cells were seeded in 96-well plates (2000 cells/well) in culture medium and incubated for 24 h and then, after culture medium removal, fresh medium containing different doses of samples treatment (0, 100, 150, 200, 250 µg/mL), and equivalent concentrations of syringic acid (20% w/w of composites quantity). Blank samples were also prepared (silica-type particles suspensions /syringic acid solution without cells) to eliminate possible interferences.

Cells were seeded in plates at a concentration of 2000 cells/well in complete culture medium (DMEM supplemented with 10% FBS and 0.1% Penicillin-Streptomycin) and incubated for 24 h under standard conditions (37°C, 5% CO_2, 95% humidity) to allow attachment. After this time, the culture medium was removed and replaced with fresh medium containing different equivalent concentrations of nanoparticles (0, 100, 150, 200, 250 µg/mL), and equivalent concentrations of syringic acid (20% w/w of the nanoparticle quantity). Blank samples were also prepared (nanoparticle/syringic acid suspensions without cells) to eliminate possible interferences.

Samples based on MSN and syringic acid were sterilized under UV irradiation (12 h), and then stock suspensions/solution of 2 mg/mL were prepared using culture medium for the solid samples and DMSO for syringic acid. Cells were incubated with particles for 72 h. After this, the culture medium containing sample was removed from the cells and replaced with medium containing 10% MTT. Cells were incubated with MTT for 1-2 hours under standard temperature and humidity conditions. After this period, the medium was removed, and the resulting crystals were dissolved in dimethyl sulfoxide. The absorbance of the supernatant was recorded at 570 nm by a Tecan plate reader. The blank absorbance was subtracted from the sample absorbance, and cell viabilities were computed relative to the negative control. Results were presented as mean value ± standard deviation.

2.6 Internalization assessment

Evaluation of the nanoparticles internalization was performed using the CytoViva hyperspectral microscopy system. It is configured to work in transmission, enhanced dark field mode (EDFM). It uses an oil-immersion condenser with patented cardioid shape, as well as illumination through an optical fiber with a liquid core, which ensures the formation of images with almost zero background, on which the details of the samples can be seen very brightly. The light scattered on these nanometric details arrives through the objective on a special video camera (Pixelfly 1392×1040 - pixel resolution, 6.45×6.45 μm pixel size, 7.3 to 13.5 fps, 5 μs-60 s exposure time range, 62% quantum efficiency), which has a spectrophotometer in front (ImSpector V10E, Specim Finland, equipped with a transmission diffraction grating). This configuration ensures 1.28 nm spectral resolution in 400-1000 nm range and 107.5 nm spatial resolution.

The settings used to record the images in which the cells and nanoparticles can be seen were: 0.8NA for 60x objective, exposure time in hundreds of milliseconds range to ensure intensities under 5000 units on each image, maximum spatial resolution and lines number. Hyperspectral images (HSI) are recorded and preprocessed under ENVI software; the first step being the lamp correction for all images following the procedure from CytoViva User Manual, Sec.6.3 [30]. This procedure removes the effects from the lamp spectrum so that sample details and spectral features are seen more clearly.

3. Results and discussion

3.1 Characterization of functionalized carriers

Small-angle X-ray diffraction was carried out to investigate the structure of pristine MCM 41, silica functionalized with boronic acid groups, MCM-B, and aminopropyl-functionalized silica, MCM-NH_2. Small-angle X-ray diffractogram

for MCM-41 shows the formation of mesoporous structure with a hexagonal pore framework, specific for this type of silica. MCM-NH_2 carrier displayed a decrease in intensity of the (100) Bragg reflection from $2\theta \cong 2°$, when compared to MCM-41, as a result of a reduction in the degree of pore array order. This effect is more pronounced in the case of MCM-B carrier, as the boronic acid functional group has larger dimensions compared to aminopropyl groups. The decrease in intensity for the (100) reflection could also be evidence for the presence of organic groups inside the silica mesopores, as the groups decrease the electron density between the silica framework and mesopore.

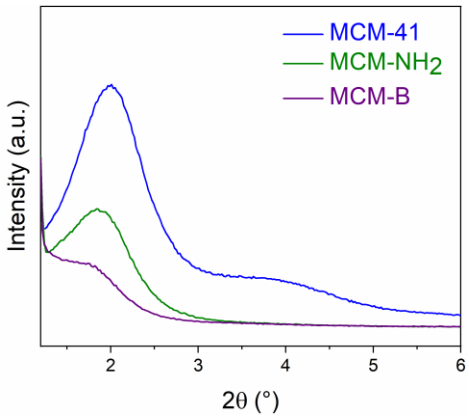

Fig 1. Small-angle XRD patterns for pristine MCM-41 and functionalized nanoparticles

FTIR spectroscopy highlights the functional moieties presence, which are bound to the silica surface. In the case of pristine silica, characteristic vibration bands of silica are observed. Symmetric and asymmetric stretching vibrations of Si-O-Si bonds are seen at 800 cm^{-1} and in the range of 1000 cm^{-1} to 1180 cm^{-1}, while the deformation and stretching vibrations of silanol groups are noticed at 460 cm^{-1} and 900 cm^{-1}, respectively. Additionally, the broad band of medium intensity in 3400-3600 cm^{-1} domain is attributed to the stretching vibrations of hydroxyl groups from silica surface. The deformation band of physically adsorbed water molecules can be observed at 1630 cm^{-1}. In the case of MCM-NH2, additional bands associated to functional groups can be noticed, such as the stretching vibrations of C-H bonds from aliphatic CH_2 groups (2980-2875 cm^{-1}), as well as deformation vibration of -NH_2 groups at 1509 cm^{-1}.

The modification of silica surface with the boronic acid derivative was also monitored by FTIR spectroscopy (Fig. 2). Thus, the vibration bands of functional groups are observed. Specifically, at 3036 cm^{-1}, the vibration band of C-H bonds of the aromatic nucleus is present. The intense asymmetric stretching vibration of C=O bond of carboxyl groups from boronic acid derivative at 1680 cm^{-1} is also observed in the sample where 4-CPBA was absorbed onto silica mesopores. This band is shifted to 1635 cm^{-1} for MCM-B and overlapping with

the vibration band of physically adsorbed water. The vibration at 1380 cm^{-1} is associated with stretching vibration of B-O bonds. The vibration band at 1530 cm^{-1} is associated with bending vibration of N-H bond from amide group, being shifted compared to that in MCM-NH_2. The stretching vibrations of hydroxyl groups bound to the boron atom are present as a shoulder at 3200 cm^{-1} in the broad characteristic silica vibration band due to hydroxyl groups. The binding of boronic acid-derivative was also confirmed by the smaller specific surface area of MCM-B (104 m^2/g) and the decrease in pore volume to 0.39 cm^3/g compared to pure silica (887 m^2/g and 0.89 cm^3/g, respectively) [17].

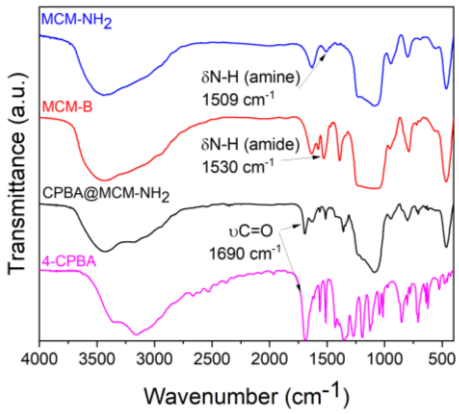

Fig. 2. FTIR spectra of functionalized MCM-41 samples and for 4-carboxyphenylboronic acid.

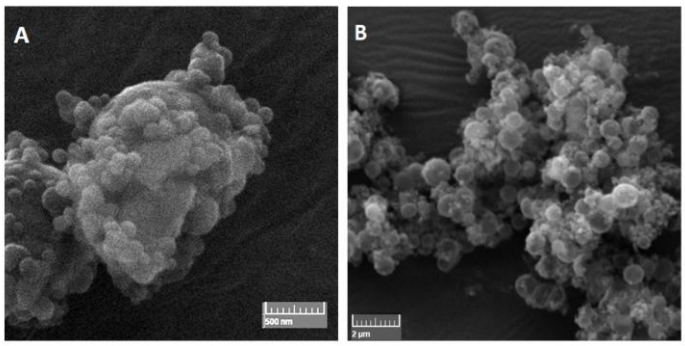

Fig. 3. SEM micrographs of functionalized carriers: A–MCM-NH_2, B–MCM-B.

The morphology of silica particles functionalized with aminopropyl groups, and respectively with the boronic acid derivative, was investigated through scanning electron microscopy (Fig. 3). Both samples display spherical particles, with an agglomeration tendency.

Thermal analysis (DTA-TG) of MCM-B carrier (Fig. 4) revealed an endothermic effect associated with a mass loss of 4.2% attributed to the evaporation of the adsorbed water, followed by two sharp exothermic effects

caused by the combustion of organic groups, at 310°C and 390°C, respectively, followed by a weaker exothermic effect at 552°C. The total mass loss associated with the exothermic effects was 19.6%. Boronic acid derivative decomposition in the same conditions leads to a residue of 25.7% at 800°C (Fig. 4).

The DTA curve of the MCM-NH_2 carrier exhibits an endothermic event associated with a mass loss of 4.1% attributed to the desorption of water from the functionalized silica mesopores, followed by two main exothermic events associated to the decomposition of aminopropyl groups. The maximum rate of decomposition is lower compared to the MCM-B carrier, occurring at 287°C and 325°C. The total loss associated with the exothermic effects is 19.1% (Fig. 4).

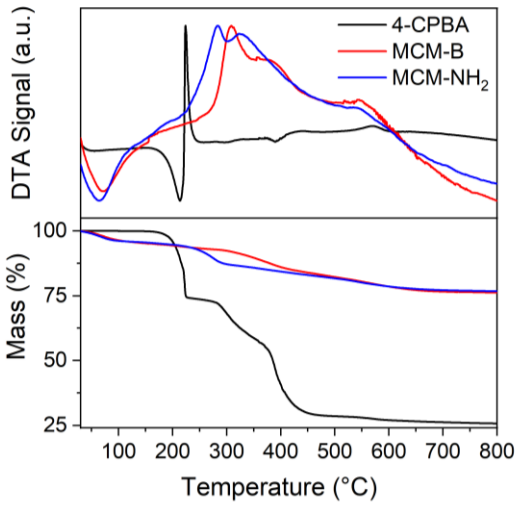

Fig. 4. Thermogravimetric analysis of functionalized carries

3.2 Characterization of composites containing syringic acid

X-ray diffraction shows that syringic acid is mostly found in the pores of the support adsorbed in amorphous state (Fig. 5A). In the case of boronic acid derivative-functionalized silica, a small diffraction peak at ~25° (2θ) can be observed, associated with a small amount of crystalline syringic acid, probably because its low total pore volume.

FTIR spectroscopy evidenced the presence of syringic acid molecules in the considered silica supports. In the case of syringic acid-loaded MCM-B support, the vibration bands characteristic to syringic acid can be observed at 1680 cm^{-1}, 1531 cm^{-1} (assigned to carboxyl groups), 1460 cm^{-1} (attributed to the deformation vibration of the C-H bond of methoxy groups), and 691 cm^{-1}, assigned to the out-of-plane deformation of phenolic groups (Fig. 5B).

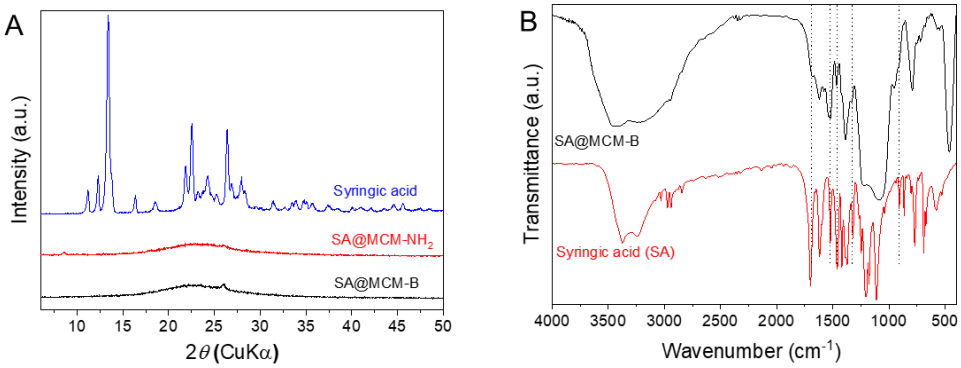

Fig. 5. Wide-angle XRD patterns of syringic acid-loaded mesoporous silica-type carriers (A) and FTIR spectra of syringic acid and SA@MCM-B sample

3.3 Release profiles of syringic acid from silica-type carriers

From both MCM-41 supports, syringic acid displays a fast release profile (Fig. 6), exhibiting a pronounced burst effect. The release profile was faster than the solubilization of crystalline syringic acid in the release medium, indicating that being a small molecule in amorphous state into mesopores of the silica carrier, it did not exhibit strong interactions with the carriers. Syringic acid is completely released after 3h.

There is no important difference in the release profile among the two samples. Therefore, the sample containing boronic acid groups was further tested *in vitro*, as the boronic acid derivative is a promising functional group that can be used for targeting tumoral cells.

Table 1

Kinetic parameters of the release profiles of syringic acid-loaded samples

Sample	k_{diff}, $10^3 min^{-1}$	k_{des}, $10^3 min^{-1}$	k_{ads}, $10^3 min^{-1}$	ΔG, $10^{21} J$	R^2	Cumulative release after 24 h, (%)
SA*	25.94	6.97	3.89	2.50	0.9998	98.92
SA@MCM-NH_2	33.64	0.94	0.03	14.78	0.9983	99.58±0.67
SA@MCM-B	40.60	5.91	0.10	17.46	0.9998	99.95±1.11

*Kinetic parameters for SA are displayed only for comparison, with no physical significance.

Both syringic acid delivery profiles were fitted by three-parameter model [31] and the kinetic parameters are shown in Table 1.

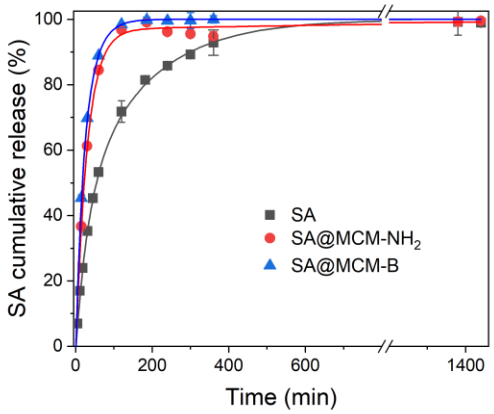

Fig. 6. Release profiles of syringic acid-loaded samples in PBS pH 5.5

This model can be used to better explain the dissolution processes from porous matrices, as it assigns a physical meaning to the kinetic parameters as follows: k_{diff} is proportional to the rate of the burst stage, k_{des} is directly proportional to the rate in the sustained release stage, and the adsorption-desorption equilibrium is described by the value of free molar energy, ΔG, that determined the amount of released biologically active compound in the burst stage. The diffusion constant is much larger than k_{des} and k_{ads} for both carriers, suggesting that syringic acid release is mostly achieved through diffusion. The rate constants of desorption are larger than those of adsorption in both cases, suggesting weak interactions between the carrier's surface and phenolic acid. ΔG has similar values for both carriers, showing that a large amount of natural compound was delivered in the burst stage.

3.4 Cytotoxicity assessment

The biocompatibility against human BJ fibroblasts was evaluated for MCM-B, CPBA@MCM-NH_2 and SA@MCM-B. The silica carrier functionalized with 4-CPBA, MCM-B, had a biocompatible behaviour on BJ dermal cell line after 72 h incubation time (Fig. 7A), with cellular viability greater than 80 % for all tested concentrations, in the range of 100-250 μg/mL. The sample containing syringic acid, SA@MCM-B, did not exhibit toxicity to healthy cells, either. The presence of the phenylboronic acid loaded on MCM-NH_2 silica pores (CPBA@MCM-NH_2) did not induce significant cytotoxic effects (Fig. 8a) in the tested concentration range (100-250 μg/mL).

BT474 ductal breast cancer cells exposed to CPBA@MCM-NH_2 and MCM-B nanoparticles showed a decreased of cell viability after 72 h incubation directly proportional to the treatment dose increasing, with a more pronounced effect for CPBA@MCM-NH_2, probably because of the presence of a larger

quantity of CPBA (Fig. 8B). Syringic acid adsorption into MCM-B enhanced cytotoxicity effect of syringic acid (statistically significant from 200 µg/mL). Cell viability decreased with increasing the concentration of SA@MCM-B, (72 % at maximum concentration), but the effect was not statistically significant. By incorporating SA into MCM-B carrier, its antiproliferative effect against breast cancer cells significantly increased.

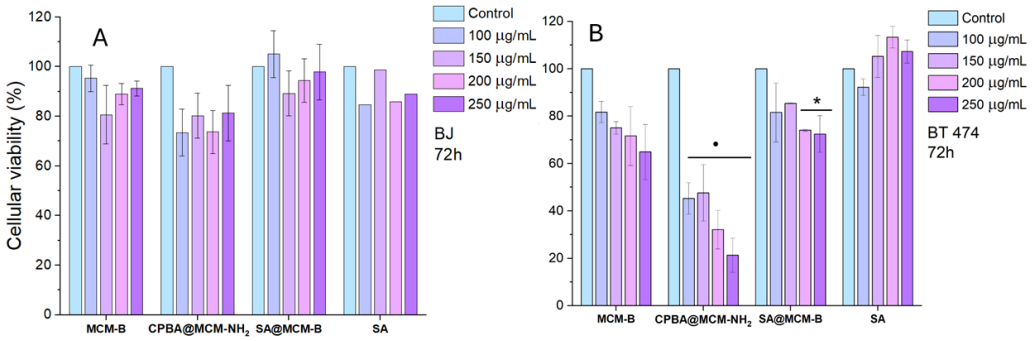

Fig. 7. Biocompatibility on BJ human dermal fibroblasts (A) and cytotoxicity on BT474 ductal breast carcinoma (B) of MCM-B, CPBA@MCM-NH_2, SA-loaded MCM-B and syringic acid alone, after 72 h incubation time; (* significant for $p < 0.05$ compared to syringic acid, • significant for $p < 0.05$ compared to control)

3.5 Assessment of nanoparticles internalization into the cell lines

The samples internalization into cells was studied on BJ fibroblasts and BT 474 ductal breast carcinoma cells, in their natural environment, without any chemical markers, after 24 h incubation of the cells with sample particles.

Fig. 9 shows the hyperspectral images obtained for CPBA@MCM-NH_2, MCM-B and SA@MCM-B cells. In the case of BJ fibroblasts, cells are mainly isolated on the glass slides, the nanoparticles are uniformly distributed within the cytoplasm, they did not enter the nucleus and did not accumulate either at the membrane edge or at the nuclear border in the endoplasmic reticulum. It was also observed that some cells did not internalize the particles. In the case of BT 474 cell line, cells grow in colonies, most of the cells internalized the nanoparticles, and the particles did not enter the nucleus or accumulate either at the membrane edge or at the nuclear border in the endoplasmic reticulum. This suggests a better internalization of the particles on the cancer cell line, which could be attributed to the targeting capacity of 4-carboxyphenylboronic acid.

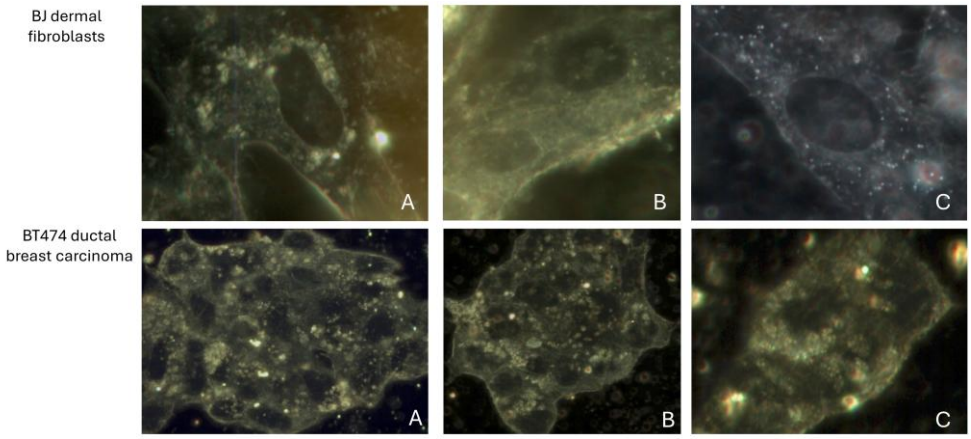

Fig. 9. Hyperspectral images of BJ dermal fibroblasts and BT 474 ductal breast carcinoma cell lines showing the Internalization of nanoparticles (white dots): A–CPBA@MCM-NH_2, B-MCM-B, C–SA@MCM-B.

6. Conclusions

MCM-41-type mesoporous silica was functionalized using 4-carboxyphenylboronic acid and then loaded with syringic acid resulting in a composite material with 20 %(wt) phenolic acid content. The release profile of syringic acid from boronic acid-functionalized support showed a fast delivery, probably because of weak interactions with the carrier's surface. *In vitro* cytotoxicity tests of syringic acid-loaded sample displayed a good biocompatibility on BJ dermal fibroblasts for all tested concentrations. The cytotoxicity on breast cancer cells increased with increasing the treatment dose, with significantly larger effects at 200 and 250 µg/mL, compared to free syringic acid. Samples containing boronic acid-derivative and syringic acid were better internalized by cancerous cells, which could be attributed to 4-carboxyphenylboronic acid targeting capacity.

Acknowledgment: This study was funded by UEFISCDI National Funding Agency (Romania) through the project no 576PED/2022.

R E F E R E N C E S

[1] *M. Capasso, M. Franceschi, K.I. Rodriguez-Castro, P. Crafa, G. Cambiè, C. Miraglia, A. Barchi, A. Nouvenne, G. Leandro, T. Meschi, G.L. De' Angelis, F. Di Mario*, Epidemiology and risk factors of pancreatic cancer, Acta Biomed 89 (2018) 141–146. https://doi.org/10.23750/ABM.V89I9-S.7923.

[2] *Y.S. Sun, Z. Zhao, Z.N. Yang, F. Xu, H.J. Lu, Z.Y. Zhu, W. Shi, J. Jiang, P.P. Yao, H.P. Zhu*, Risk Factors and Preventions of Breast Cancer, Int J Biol Sci 13 (2017) 1387. https://doi.org/10.7150/IJBS.21635.

[3] *P. Vineis, C.P. Wild*, Global cancer patterns: Causes and prevention, The Lancet 383 (2014) 549–557. https://doi.org/10.1016/S0140-6736(13)62224-2.

[4] *M. Abotaleb, A. Liskova, P. Kubatka, D. Büsselberg*, Therapeutic Potential of Plant Phenolic Acids in the Treatment of Cancer, Biomolecules 2020, Vol. 10, Page 221 10 (2020). https://doi.org/10.3390/BIOM10020221.

[5] *R. Rani, P. Malik, S. Dhania, T.K. Mukherjee*, Recent Advances in Mesoporous Silica Nanoparticle-Mediated Drug Delivery for Breast Cancer Treatment, Pharmaceutics 2023, Vol. 15, Page 227 15 (2023) 227. https://doi.org/10.3390/PHARMACEUTICS15010227.

[6] *Z. Edis, J. Wang, M.K. Waqas, M. Ijaz, M. Ijaz*, Nanocarriers-mediated drug delivery systems for anticancer agents: An overview and perspectives, Int J Nanomedicine 16 (2021) 1313–1330. https://doi.org/10.2147/IJN.S289443.

[7] *A. Watermann, J. Brieger*, Mesoporous Silica Nanoparticles as Drug Delivery Vehicles in Cancer, Nanomaterials 2017, Vol. 7, Page 189 7 (2017) 189. https://doi.org/10.3390/NANO7070189.

[8] *A. Almomen, A. Alhowyan*, A Comprehensive Study on Folate-Targeted Mesoporous Silica Nanoparticles Loaded with 5-Fluorouracil for the Enhanced Treatment of Gynecological Cancers, J Funct Biomater 15 (2024) 74. https://doi.org/10.3390/JFB15030074/S1.

[9] *L. Yang, H. Li, A. Luo, Y. Zhang, H. Chen, L. Zhu, D. Yang*, Macrophage membrane-camouflaged pH-sensitive nanoparticles for targeted therapy of oral squamous cell carcinoma, J Nanobiotechnology 22 (2024) 1–16. https://doi.org/10.1186/S12951-024-02433-4/FIGURES/8.

[10] *Y. Dutta Gupta, Y. Mackeyev, S. Krishnan, S. Bhandary*, Mesoporous silica nanotechnology: promising advances in augmenting cancer theranostics, (n.d.). https://doi.org/10.1186/s12645-024-00250-w.

[11] *A. Matadamas-Ortiz, J.F. Pérez-Robles, R. Reynoso-Camacho, S.L. Amaya-Llano, A. Amaro-Reyes, P. Di Pierro, C. Regalado-González*, Effect of Amine, Carboxyl, or Thiol Functionalization of Mesoporous Silica Particles on Their Efficiency as a Quercetin Delivery System in Simulated Gastrointestinal Conditions, Foods 2024, Vol. 13, Page 1208 13 (2024) 1208. https://doi.org/10.3390/FOODS13081208.

[12] *T. Miyazaki, T. Khan, Y. Tachihara, M. Itoh, T. Miyazawa, T. Suganami, Y. Miyahara, H. Cabral, A. Matsumoto*, Boronic Acid Ligands Can Target Multiple Subpopulations of Pancreatic Cancer Stem Cells via pH-Dependent Glycan-Terminal Sialic Acid Recognition, ACS Appl Bio Mater 4 (2021) 6647–6651. https://doi.org/10.1021/acsabm.1c00383.

[13] *M. Ghosh, P. Hazarika, S.J. Dhanya, D. Pooja, H. Kulhari*, Exploration of sialic acid receptors as a potential target for cancer treatment: A comprehensive review, Int J Biol Macromol 257 (2024) 128415. https://doi.org/10.1016/J.IJBIOMAC.2023.128415.

[14] *H. Kim, S.J. Kang, W.J. Rhee*, Phenylboronic Acid-conjugated Exosomes for Enhanced Anticancer Therapeutic Effect by Increasing Doxorubicin Loading Efficiency, Biotechnology and Bioprocess Engineering 26 (2021) 78–85. https://doi.org/10.1007/S12257-020-0107-5/METRICS.

[15] *Y. Xu, Y. Huang, W. Lu, S. Liu, Y. Xiao, J. Yu*, 4-Carboxyphenylboronic acid-decorated, redox-sensitive rod-shaped nano-micelles fabricated through co-assembling strategy for active targeting and synergistic co-delivery of camptothecin and gemcitabine, European Journal of Pharmaceutics and Biopharmaceutics 144 (2019) 193–206. https://doi.org/10.1016/J.EJPB.2019.09.019.

[16] *S. Ghosh, M. Kundu, S. Dutta, S. Mahalanobish, N. Ghosh, J. Das, P.C. Sil*, Enhancement of anti-neoplastic effects of cuminaldehyde against breast cancer via mesoporous silica nanoparticle based targeted drug delivery system, Life Sci 298 (2022). https://doi.org/10.1016/j.lfs.2022.120525.

[17] *M. Deaconu, A.M. Prelipcean, A.M. Brezoiu, R.A. Mitran, G. Isopencu, C. Matei, D. Berger*, Novel Collagen-Polyphenols-Loaded Silica Composites for Topical Application, Pharmaceutics 15 (2023) 312. https://doi.org/10.3390/PHARMACEUTICS15020312/S1.

[18] *A.M. Brezoiu, L. Bajenaru, D. Berger, R.A. Mitran, M. Deaconu, D. Lincu, A.S. Guzun, C. Matei, M.G. Moisescu, T. Negreanu-Pirjol*, Effect of Nanoconfinement of Polyphenolic Extract from Grape Pomace into Functionalized Mesoporous Silica on Its Biocompatibility and Radical

Scavenging Activity, Antioxidants 2020, Vol. 9, Page 696 9 (2020) 696. https://doi.org/10.3390/ANTIOX9080696.

[19] *P. Zhang, B. Sun, J. Tong, G. Xia, J. Zhang, C. Li, W. Yang*, Polyphenols Extracted from Enteromorpha clathrata Induce Apoptosis in Hepa1-6 Cell by Activating the Mitochondrial Apoptosis Signaling Pathways, Journal of Ocean University of China 22 (2023) 1393–1402. https://doi.org/10.1007/S11802-023-5498-4/METRICS.

[20] *C. Srinivasulu, M. Ramgopal, G. Ramanjaneyulu, C.M. Anuradha, C. Suresh Kumar*, Syringic acid (SA) – A Review of Its Occurrence, Biosynthesis, Pharmacological and Industrial Importance, Biomedicine and Pharmacotherapy 108 (2018) 547–557. https://doi.org/10.1016/j.biopha.2018.09.069.

[21] *S.J. Ha, J. Lee, J. Park, Y.H. Kim, N.H. Lee, Y.E. Kim, K.M. Song, P.S. Chang, C.H. Jeong, S.K. Jung*, Syringic acid prevents skin carcinogenesis via regulation of NoX and EGFR signaling, Biochem Pharmacol 154 (2018) 435–445. https://doi.org/10.1016/j.bcp.2018.06.007.

[22] *A. Mihanfar, S.G. Darband, S. Sadighparvar, M. Kaviani, M. Mirza-Aghazadeh-Attari, B. Yousefi, M. Majidinia*, In vitro and in vivo anticancer effects of syringic acid on colorectal cancer: Possible mechanistic view, Chem Biol Interact 337 (2021). https://doi.org/10.1016/j.cbi.2020.109337.

[23] *M. Abotaleb, A. Liskova, P. Kubatka, D. Büsselberg*, Therapeutic Potential of Plant Phenolic Acids in the Treatment of Cancer, Biomolecules 2020, Vol. 10, Page 221 10 (2020) 221. https://doi.org/10.3390/BIOM10020221.

[24] *L. Zhang, X. La, J. Tian, H. Li, A. Li, Y. Liu, C. Wu, Z. Li*, The phytochemical vitexin and syringic acid derived from foxtail fillet bran inhibit breast cancer cells proliferation via GRP78/SREBP-1/SCD1 signaling axis, J Funct Foods 85 (2021). https://doi.org/10.1016/j.jff.2021.104620.

[25] *J. Muthukumaran, S. Srinivasan, R.S. Venkatesan, V. Ramachandran, U. Muruganathan*, Syringic acid, a novel natural phenolic acid, normalizes hyperglycemia with special reference to glycoprotein components in experimental diabetic rats, Journal of Acute Disease 2 (2013) 304–309. https://doi.org/10.1016/s2221-6189(13)60149-3.

[26] *A.P. Dalmagro, A. Camargo, A.L.B. Zeni*, Morus nigra and its major phenolic, syringic acid, have antidepressant-like and neuroprotective effects in mice, Metab Brain Dis 32 (2017) 1963–1973. https://doi.org/10.1007/s11011-017-0089-y.

[27] *M. Lavanya, R. Krishnamoorthy, M.A. Alshuniaber, S. Manoharadas, C. Perumal Palanisamy, V. Priya Veeraraghavan, S. Jayaraman, P. Rajagopal, R. Padmini*, Formulation, characterization and evaluation of gelatin-syringic acid/zinc oxide nanocomposite for its effective anticancer, antioxidant and anti-inflammatory activities, J King Saud Univ Sci 35 (2023) 102909. https://doi.org/10.1016/J.JKSUS.2023.102909.

[28] *M. Mihailescu, L.C. Miclea, A.M. Pleava, N. Tarba, E.N. Scarlat, R.D. Negoita, M.G. Moisescu, T. Savopol*, Method for nanoparticles uptake evaluation based on double labeled fluorescent cells scanned in enhanced darkfield microscopy, Biomed Opt Express 14 (2023) 2796. https://doi.org/10.1364/BOE.490136.

[29] *S. Ioniță, R.-C. Popescu, I.N. Irimescu, M. Deaconu, N. Tarbă, C. Matei, M. Mihailescu, D.-I. Savu, D. Berger*, Role of mesoporous silica functionalized with boronic acid derivative in targeted delivery of doxorubicin and co-delivery of doxorubicin and resveratrol, Microporous and Mesoporous Materials 375 (2024) 113176. https://doi.org/10.1016/J.MICROMESO.2024.113176.

[30] Hyperspectral Microscope User Manual Illuminating the Future, (n.d.). www.cytoviva.com (accessed June 5, 2024).

[31] *L. Zeng, L. An, X. Wu*, Modeling Drug-Carrier Interaction in the Drug Release from Nanocarriers, J Drug Deliv 2011 (2011) 370308. https://doi.org/10.1155/2011/370308.